Gas Sensors

Nonaqueous Synthesis of Nanocrystalline Semiconducting Metal Oxides for Gas Sensing**

Nicola Pinna, Giovanni Neri, Markus Antonietti, and Markus Niederberger**

Air pollution is one of the emerging problems in our society. The more and more strict regulations on the emission of toxic gases require fast and accurate detection at sub-ppm concentrations. Among these gases, carbon monoxide and nitrogen oxides are the major atmospheric pollutants. In Europe, for example, the alarm thresholds are about 10 ppm for CO and 0.1 ppm for NO_2. Sensing devices based on metal oxide semiconductors are mainly used for the detection of these gases. When a metal oxide is exposed to reducing or oxidizing gases, its resistance varies in accordance with the gas concentration. The theory for the operation of such sensors involves absorption/desorption phenomena and reactions at the surface of the metal oxide. Materials with high surface areas are advantageous for obtaining a good sensitivity in sensing applications. Indeed it was demonstrated that a decrease in the size of the crystallite in the sensing layer leads to a considerable increase in sensitivity.[1]

[*] Dr. N. Pinna, Prof. Dr. M. Antonietti, Dr. M. Niederberger
Max-Planck-Institute of Colloids and Interfaces
14424 Potsdam (Germany)
Fax: (+49) 331-567-9502
E-mail: pinna@mpikg-golm.mpg.de
markus.niederberger@mpikg-golm.mpg.de

Prof. Dr. G. Neri
University of Messina
Department of Industrial Chemistry and Materials Engineering
98166 Messina (Italy)

[**] Financial support by the Max-Planck Society is gratefully acknowledged. We thank the Fritz-Haber Institute and Prof. R. Schlögl for the use of the electron microscope, and Klaus Weiss for his technical assistance.

 DOI: 10.1002/ange.200460610

Sol–gel procedures based on the hydrolysis and condensation of metal halide or metal alkoxide precursors in aqueous solution have been applied extensively to prepare thin films suitable for sensing applications.[2,3] However, the approach involving direct deposition of preformed nanopowders onto the substrates of the micropatterned sensors has been less explored.[4–7] This latter approach is highly versatile because it permits the large-scale production of the sensor devices by simply depositing the prefabricated metal oxide particles onto the sensor substrates.

We reported recently a halide- and surfactant-free nonaqueous route to control the particle size, shape, and crystallinity of nanocrystalline perovskites and related compounds.[8] The successful preparation of V_2O_3, Nb_2O_5, Ta_2O_5, and HfO_2 nanoparticles gave further evidence for the wide applicability of this approach.[9–11]

Herein we present a nonaqueous synthesis of nanocrystalline SnO_2 and In_2O_3. The SnO_2, in particular, was obtained in a previously non-accessible small particle size and crystal quality. These two metal oxides are particularly interesting for sensing applications. SnO_2 shows good sensitivity to reducing gas (for example, CO)[12] and In_2O_3 to oxidizing ones (for example, NO_2)[13,14] depending, among other parameters, on the method of preparation and crystallite size.[15,16] To investigate the sensing characteristics of the as-synthesized nanocrystals, they were deposited without addition of any binder or activation layers on a micropatterned alumina substrate and tested for their ability to detect trace levels of NO_2, CO, and CH_4 in air.

The X-ray powder diffraction (XRD) patterns of the as-synthesized nanoparticles are shown in Figure 1. The XRD pattern of pure SnO_2 (Figure 1a) displays four main broad peaks arising from the very small cristallite size and can be attributed to the Cassiterite structure (JCPDS 41-1445). This assignment is further confirmed by diffraction patterns calculated from the Debye scattering equation[17,18] for spherical, monodisperse particles with diameters of 2.2 nm (Figure 1a dotted line). The calculated and experimental patterns are in good agreement. The XRD pattern of the In_2O_3 nanoparticles (Figure 1b) shows sharp peaks corresponding to the In_2O_3 cubic structure (JCPDS 6-416). The sharpness of the peaks indicates a much larger particle size compared to SnO_2.

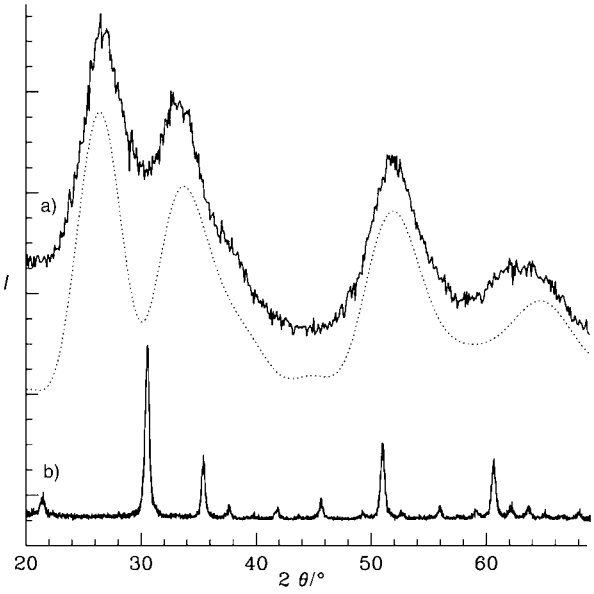

Figure 1. X-ray powder diffraction patterns of the as-synthesized SnO_2 (a), and In_2O_3 (b) nanoparticles. The Debye scattering equation calculated for 2.2-nm spherical SnO_2 nanoparticles is shown as a dotted line.

Figure 2a shows a high-resolution transmission electron micrograph (HRTEM) of an assembly of SnO_2 nanoparticles with an average size of 2–2.5 nm, which is in good agreement

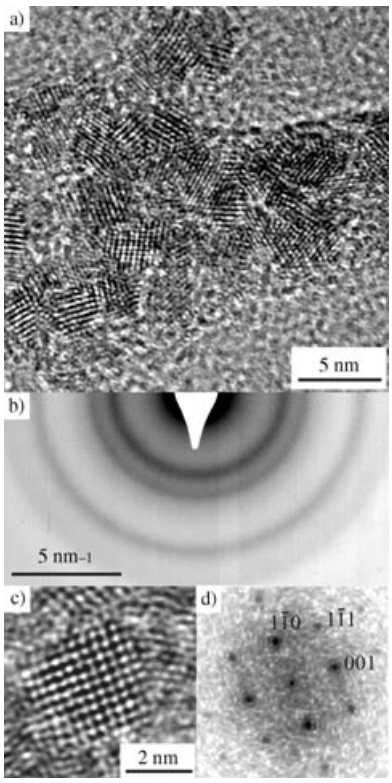

Figure 2. HRTEM image of an assembly of SnO_2 nanoparticles (a), selected-area electron diffraction (b), HRTEM image of an isolated nanoparticle (c), and its PS (d).

with the XRD data. Each particle presents well-defined lattice fringes which indicate that the particles are highly crystallized even at such a small size. The lack of any surface-protecting layers results in some agglomeration of the particles. The randomly oriented lattice fringes show the particles are neither coalesced nor do they show epitaxial aggegration. Figure 2b shows a selected-area electron diffraction (SAED) pattern. The lattice distances measured from the diffraction rings are in perfect agreement with the Cassiterite structure. Figure 2c shows the HRTEM image of an isolated particle oriented along the [110] direction. Its power spectrum (PS; Figure 2d) provides evidence that the particle is highly crystallized and does not present any structural defaults.

Figure 3a shows a TEM image of the corresponding In_2O_3 nanoparticles. The particles have a cubelike shape with an average length of 20 nm. The SAED pattern of such an assembly (Figure 3b) shows rings, formed by many spots,

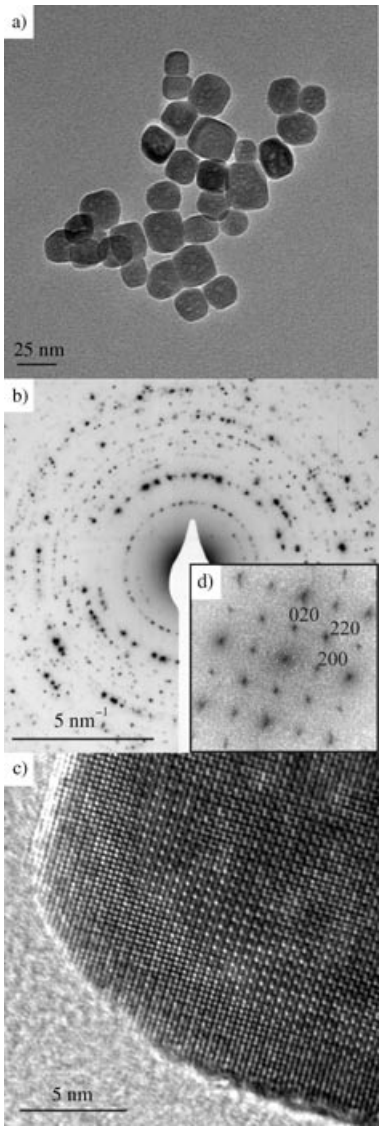

Figure 3. TEM image of an assembly of In_2O_3 nanoparticles (a), selected-area electron diffraction (b), HRTEM image of a part of a nanoparticle (c), and its PS (d).

which correspond to the In_2O_3 cubic structure. The HRTEM image (Figure 3c) of a part of one particle shows several lattice planes with perfect crystallinity. The sharp reflections of its PS can be unambiguously attributed to the In_2O_3 structure for a particle oriented along the [001] direction.

Sensors were realized from these SnO_2 and In_2O_3 nanoparticles by depositing thin films of the respective particles from an aqueous ink onto alumina substrates by a simple printing method. The mechanical and electrical properties of the deposited films were evaluated prior to the sensing tests. It is interesting to note that the sensing films without sintering are already mechanically resistant and adhere to the support. This observation is likely a consequence of the very fine particle size, which strongly improves the adhesion on the alumina surface. From an electrical point of view, the In_2O_3 sensor shows a substantially higher conductivity (around 1.8×10^{-4} A) compared to the SnO_2 sensor (3.6×10^{-9} A) in dry air at 300 °C. This result is likely related to the very small particle size of the tin dioxide, which is well below the critical grain size $d_c < 2L$ and a space-charge depth $L = 3$ nm for SnO_2, and results in the formation of an electron-depleted space charge layer extending over the whole crystallite.[19]

The sensing properties of the nanopowders towards trace levels of both oxidizing (NO_2) and reducing gases (CO, CH_4) were analyzed between 100 and 450 °C in dry air. The response of the In_2O_3 sensor to 2 ppm of NO_2 as a function of the operating temperature is shown in Figure 4a. The response to NO_2 increases with increasing temperature, with a maximum sensitivity $S = I_{air}/I_{2\,ppm\ NO_2} = 100$ around 200 °C. Figure 4b shows the dynamic response of the sensor at 250 °C to different and successive concentration pulses of NO_2 (2–20 ppm). NO_2 is an oxidizing gas and therefore causes a decrease in the conductance of n-type semiconductors. The output signals essentially recover to the initial level, thus indicating the reversibility of the interactions between the sensing elements and the gas to be detected, with a fast (less than 60 s) response time (that is, the time required to reach 90 % of the full response). Figure 4c displays the calibration curve of the sensor at 250 °C for NO_2. The experimental data were fitted by using a power-law relation expressed as:

$$S = I_{air}/I_{gas} = (1 + k\,[NO_2])^m \qquad (1)$$

where k is the sensitivity coefficient and m the power-law exponent. From the straight line obtained, we calculated $m = 0.49 \pm 0.06$ ppm^{-1} and extrapolated a lower detection limit of about 1 ppb for NO_2 in air. Our results show a remarkable increase in sensitivity (between two and ten times) with respect to the In_2O_3-based NO_2 sensors reported in the recent literature.[13,14,16,20,21] However, in these cases the sensing layers were prepared by different methods.

An additional advantage of our sensor is that cross-sensitivity tests with CO and CH_4 have shown that it does not show an appreciable response to reducing gases between 100–300 °C, thus making it highly selective towards the detection of nitrogen dioxide.

A good response for the reducing gases was observed with both the In_2O_3 and SnO_2 sensors at temperatures higher than 400 °C. This behavior is typical for metal oxides, which generally require the presence of suitable metal promoters to decrease the operating temperature substantially.[22] As an example, Figure 5 reports the dynamic response of the SnO_2 sensor at 400 °C towards different CO concentrations (10–100 ppm) in dry air.

In conclusion the successful synthesis of semiconducting metal oxide nanocrystals of SnO_2 and In_2O_3 by using a nonaqueous approach involving the reaction of a metal alkoxide with benzyl alcohol is presented. The products were obtained in the form of fine nanocrystalline powders that had superior crystallinity and good yields which permits them to

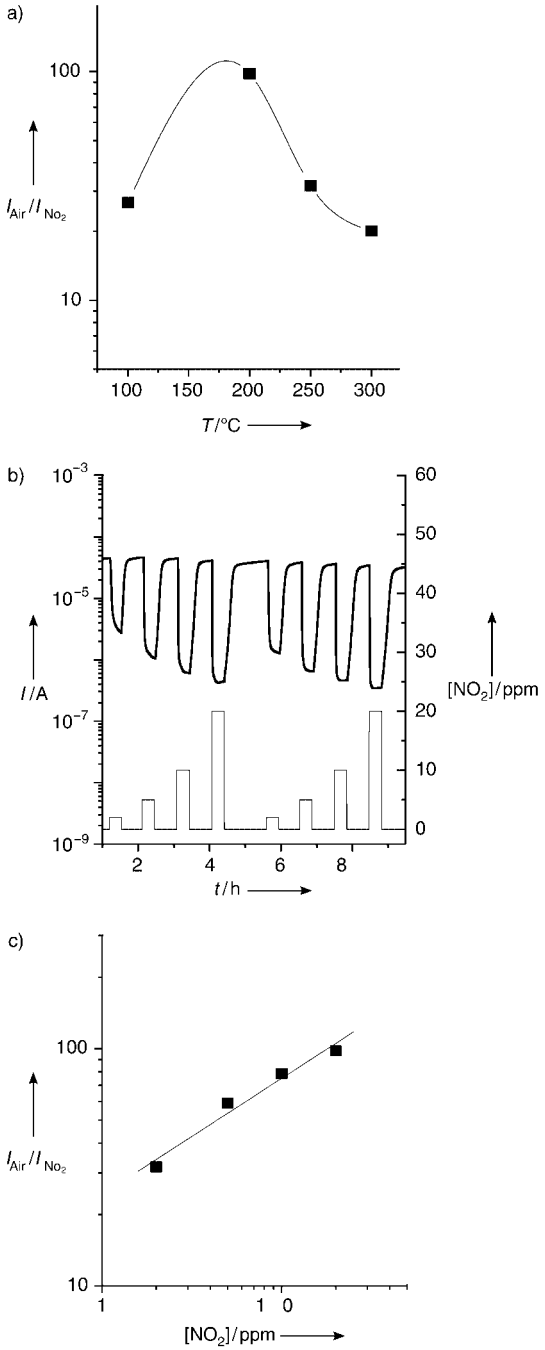

Figure 4. Response to 2 ppm of NO_2 versus operating temperature of the In_2O_3 sensor (a), its dynamic response at 250 °C (b), and calibration curve at 250 °C (c).

be used for sophisticated applications in customer-near devices, for example, as conducting glass coatings, for IR filters, or in sensors. The nanopowders can be used directly to fabricate sensor devices just by deposition of the as-synthesized nanoparticles onto micropatterned alumina substrates. Both metal oxides showed high sensitivity and good recovery time. Indium oxide, in particular, showed an unusual high sensitivity to NO_2 (namely, 1 ppb) at low temperature as well as the essential selectivity against CO and methane required by high technological applications.

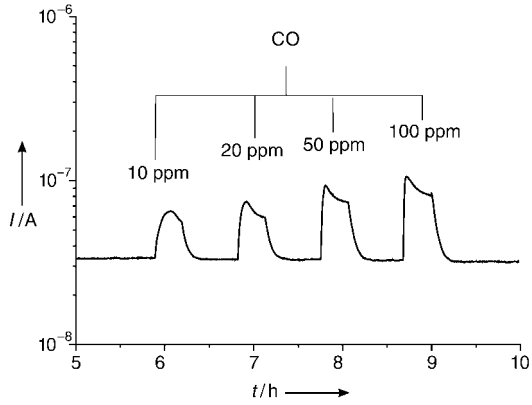

Figure 5. Dynamic response of the SnO_2 sensor at 400 °C to trace levels of CO in air.

Experimental Section

Synthesis: All the synthetic procedures were carried out in a glovebox (O_2 and $H_2O < 0.1$ ppm). In a typical synthesis of nanoparticles, tin(IV) *tert*-butoxide (500 mg, 1.216 mmol) or indium(III) isopropoxide (200 mg, 0.685 mmol) was added to benzyl alcohol (20 mL). The reaction mixture was transferred into a teflon cup of 45 mL inner volume, placed in a steel autoclave, and carefully sealed. The autoclave was taken out of the glovebox and heated in a furnace at 220 °C for 2 days. The resulting milky suspensions were centrifuged, the precipitates thoroughly washed with ethanol and dichloromethane, and subsequently dried in air at 60 °C.

Characterization: For TEM studies one or more drops of the solution of the nanoparticles dispersed in ethanol were deposited on the amorphous carbon film. A Philips CM200 FEG microscope, 200 kV, equipped with a field emission gun was used. The coefficient of spherical aberration was $C_s = 1.35$ mm. The X-ray powder diffraction (XRD) patterns of all samples were measured in reflection mode ($Cu_{K\alpha}$ radiation) on a Bruker D8 diffractometer equipped with a scintillation counter.

Sensing tests: These were carried out on sensors prepared by depositing thin films of the nanopowders dispersed in water onto alumina substrates (3×3 mm^2) at a thickness of around 1 μm. The substrates were fitted, on the front side, with gold interdigitated contacts and, on the backside, with a Pt heater. The sensors were bound as suspended devices onto TO-8 supports and introduced in a teflon test chamber for testing their sensitivity to CO, CH_4, and NO_2 in a controlled atmosphere. The gases coming from certified bottles were further diluted in air and their concentration was varied by a gas-mixing system (MKS mod. 647B) and different mass-flow controllers (MFCs). The experiments were carried out by measuring the electrical current of the sensor devices under a voltage of 1 V by an electrometer (Keithley mod. 6517A). A personal computer with LABview software controlled all the operations related to the gas protocol and to data acquisition, storage, and plotting in real time through a GPIB interface. The sensor response was defined as I_{air}/I_{gas} for NO_2 detection and I_{gas}/I_{air} for CO and CH_4 detection, where I_{air} is the electrical current of the film in air and I_{gas} is the electrical current under gas flow.

Received: May 10, 2004 [Z460610]
Published Online: June 28, 2004

Keywords: gas sensors · indium · nanoparticles · synthetic methods · tin

[1] N. Yamazoe, *Sens. Actuators B* **1991**, *5*, 7.
[2] R. Rella, P. Siciliano, S. Capone, M. Epifani, L. Vasanelli, A. Licciulli, *Sens. Actuators B* **1999**, *58*, 283.
[3] S. Shukla, S. Seal, L. Ludwig, C. Parish, *Sens. Actuators B* **2004**, *97*, 256.
[4] P. Fau, M. Sauvan, S. Trautweiler, C. Nayral, L. Erades, A. Maissonat, B. Chaudret, *Sens. Actuators B* **2001**, *78*, 83.
[5] K. Soulantica, L. Erades, M. Sauvan, F. Senocq, A. Maissonat, B. Chaudret, *Adv. Funct. Mater.* **2003**, *13*, 553.
[6] Y. Wang, X. Jiang, Y. Xia, *J. Am. Chem. Soc.* **2003**, *125*, 16176.
[7] M. Law, H. Kind, B. Messer, F. Kim, P. Yang, *Angew. Chem.* **2002**, *114*, 2511; *Angew. Chem. Int. Ed.* **2002**, *41*, 2405.
[8] M. Niederberger, N. Pinna, J. Polleux, M. Antonietti, *Angew. Chem.* **2004**, *116*, 2320; *Angew. Chem. Int. Ed.* **2004**, *43*, 2270.
[9] N. Pinna, M. Antonietti, M. Niederberger, *Colloids Surf. A* **2004**, in press.
[10] N. Pinna, G. Garnweitner, M. Antonietti, M. Niederberger, *Adv. Mater.* **2004**, in press.
[11] M. Antonietti, M. Niederberger, N. Pinna, Deutsche Patentanmeldung Nr. 10 2004 016 131.3, **2004**.
[12] N. Yamazoe, Y. Kurokawa, T. Seiyama, *Sens. Actuators* **1983**, *4*, 283.
[13] A. Gurlo, N. Bârsan, M. Ivanovskaya, U. Weimar, W. Göpel, *Sens. Actuators B* **1998**, *47*, 92.
[14] M. Ivanovskaya, A. Gurlo, P. Bogdanov, *Sens. Actuators B* **2001**, *77*, 264.
[15] R. Dolbec, M. A. El Khakoni, A. M. Serventi, R. G. Saint-Jacques, *Sens. Actuators B* **2003**, *93*, 566.
[16] A. Gurlo, M. Ivanovshaya, N. Barsan, M. Schweizer-Berberich, U. Weimar, W. Gopel, A. Dieguez, *Sens. Actuators B* **1997**, *44*, 327.
[17] W. Vogel, *Cryst. Res. Technol.* **1998**, *33*, 1141.
[18] N. Pinna, U. Wild, J. Urban, R. Schlögl, *Adv. Mater.* **2003**, *15*, 329.
[19] Y. Shimizu, M. Egashira, *MRS Bull.* **1999**, *24*, 18.
[20] H. Steffes, C. Imawan, F. Solzbacher, E. Obermeier, *Sens. Actuators B* **2003**, *68*, 249.
[21] C. Cantalini, W. Wlodarski, H. T. Sun, M. Z. Atashbar, M. Passacantando, A. R. Phani, S. Santucci, *Thin Solid Films* **1999**, *350*, 276.
[22] D. Kohl, *Sens. Actuators B* **1990**, *1*, 158.

